

Roles of Synoptic to Quasi-Biweekly Disturbances in Generating the Summer 2003 Heavy Rainfall in East China

HONG-BO LIU

LASG, Institute of Atmospheric Physics, Chinese Academy of Sciences, Beijing, China

JING YANG

State Key Laboratory of Earth Surface Processes and Resource Ecology, Beijing Normal University, Beijing, China

DA-LIN ZHANG

Department of Atmospheric and Oceanic Science, University of Maryland, College Park, College Park, Maryland

BIN WANG

LASG, Institute of Atmospheric Physics, Chinese Academy of Sciences, and Center for Earth System Science, Tsinghua University, Beijing, China

(Manuscript received 7 February 2013, in final form 5 September 2013)

ABSTRACT

During the mei-yu season of the summer of 2003, the Yangtze and Huai River basin (YHRB) encountered anomalously heavy rainfall, and the northern YHRB (nYHRB) suffered a severe flood because of five continuous extreme rainfall events. A spectral analysis of daily rainfall data over YHRB reveals two dominant frequency modes: one peak on day 14 and the other on day 4 (i.e., the quasi-biweekly and synoptic-scale mode, respectively). Results indicate that the two scales of disturbances contributed southwesterly and northeasterly anomalies, respectively, to the mei-yu frontal convergence over the southern YHRB (sYHRB) at the peak wet phase. An analysis of bandpass-filtered circulations shows that the lower and upper regions of the troposphere were fully coupled at the quasi-biweekly scale, and a lower-level cyclonic anomaly over sYHRB was phase locked with an anticyclonic anomaly over the Philippines. At the synoptic scale, the strong northeasterly components of an anticyclonic anomaly with a deep cold and dry layer helped generate the heavy rainfall over sYHRB. Results also indicate the passages of five synoptic-scale disturbances during the nYHRB rainfall. Like the sYHRB rainfall, these disturbances originated from the periodical generations of cyclonic and anticyclonic anomalies at the downstream of the Tibetan Plateau. The nYHRB rainfalls were generated as these disturbances moved northeastward under the influence of monsoonal flows and higher-latitude eastward-propagating Rossby wave trains. It is concluded that the sYHRB heavy rainfall resulted from the superposition of quasi-biweekly and synoptic-scale disturbances, whereas the intermittent passages of five synoptic-scale disturbances led to the flooding rainfall over nYHRB.

1. Introduction

The Yangtze and Huai River basin (hereafter YHRB), covering roughly the area of 27°–35°N, 114°–121°E, is one of the most centralized regions over China for the warm season heavy rainfall. It is located in the extratropical

region of east China, simultaneously affected by the subtropical and mid- to high-latitude large-scale systems during summer months (Zhang et al. 2003). The summer rainfall over this region is mostly caused by the mei-yu front, low pressure systems (e.g., southwest vortex), and mesoscale convective systems (MCSs) (Zhu et al. 2000; Jiao et al. 2004; Liu et al. 2008; Zhang and Zhang 2012). The mei-yu front is characterized by weak temperature gradients but high equivalent potential temperature θ_e gradients due to the strong meridional moisture contrast. It forms as southwesterly tropical flows from warm

Corresponding author address: Dr. Yang Jing, State Key Laboratory of Earth Surface Processes and Resource Ecology, Beijing Normal University, Beijing 100875, China.
E-mail: yangjing@bnu.edu.cn

oceans meet northerly (or northeasterly) cold air from higher latitudes (Zhang et al. 2003; Ding et al. 2007). The mei-yu front and the low pressure system always bring large amounts of rainfall to YHRB from mid-June to mid-July (Ding 1994; Ding et al. 2007).

Recent studies indicate that convection activity over YHRB and the associated circulations exhibit substantial intraseasonal variability during the warm season (Chen et al. 2000; Zhang et al. 2002, 2003; Yang and Li 2003). The YHRB rainfall shows obvious 20–50-, 21–30-, and 12–20-day (quasi biweekly) periodical variations as a response to the intraseasonal variations over subtropical and mid- to high-latitude regions (Zhang et al. 2003; Mao et al. 2010; Yang et al. 2010, 2013). In addition, many of the flooding rainfall events over YHRB are associated with the extremely active phase of intraseasonal variations. For example, the severe flood over YHRB during the summer of 1998 was shown to be consistent with two intraseasonal variations occurring in June and July (Zhu et al. 2003; Wang et al. 2003; Chen et al. 2005; Liu et al. 2008). The active and break sequences of rainfall over YHRB during the summer of 1991 were also regulated by an oscillatory mode with a period of 15–35 days (Mao and Wu 2006).

The intraseasonal variation modes usually provide favorable background conditions, such as continuous moisture supply and an important cyclonic anomaly or an anticyclonic anomaly, for persistent rainfall over the YHRB region (Zhu et al. 2003; Mao and Wu 2006; Yang et al. 2010). On the other hand, individual rainfall events are often seen being associated with frequently traveling synoptic-scale weather systems in midlatitudes (Jiao et al. 2004; Qian et al. 2004; Zhang and Zhang 2012). These weather systems can also be thought of as being a succession of synoptic-time-scale (3–8 days) disturbances (i.e., cyclonic and anticyclonic anomalies) in the atmospheric circulations (Lau and Lau 1990; Berry et al. 2012). Previous studies have focused mostly on the synoptic-scale disturbances occurring over tropical to subtropical ocean regions because of the wide interests in tropical cyclones (Lau and Lau 1990, 1992; Chen and Weng 1998; Gu and Zhang 2001; Chang et al. 2005; Tam and Li 2006). In addition, these disturbances interact closely with tropical deep convection. For example, Gu and Zhang (2002) noted that the mean distributions and annual cycles of westward-propagating synoptic-scale disturbances match well those of the intertropical convergence zone (ITCZ).

In contrast, only limited work has been done to examine the effects of synoptic-scale disturbances on the development of midlatitude convective systems. Recently, Berry et al. (2012) found that on average one synoptic-scale disturbance moves across the Australian

monsoon region every 2.5 days during the Southern Hemispheric summer, which account for 40%–50% of the summer rainfall. Unfortunately, few such studies have been conducted to examine the relationship between such disturbances and persistent warm season rainfall (e.g., along the mei-yu front) at midlatitudes in the Northern Hemisphere.

In the summer of 2003, YHRB was buffeted by a string of continuous rainstorm episodes, and a total of five intense rainfall events caused a severe flood over the Huai River basin during the mei-yu season (Jiao et al. 2004). The basin experienced positive rainfall anomalies of more than 12 mm day^{-1} with respect to the 10-yr (i.e., 2000–09) daily rainfall average (not shown). Compared to the other two flooding rainfall years (i.e., 2005 and 2007), the summer 2003 rainfall over YHRB was characterized by persistent and intense rainfall events, with rainfall standard deviations of 11.84, 8.76, and 8.29 mm day^{-1} for 2003, 2005, and 2007, respectively. Thus, this flood disaster was the most serious case in terms of the number of lost lives and cost of the property damage among the three flooding events in the respective years of 2003, 2005, and 2007. Many studies have been carried that examined the favorable large-scale background circulations (e.g., blocking high, western Pacific subtropical high) and moisture transport characteristics for the summer 2003 heavy rainfall (Jiao et al. 2004; Sun et al. 2004; Zhou et al. 2005). Results showed that the quasi-stationary western Pacific subtropical high and its more southward location were partly responsible for the continuous intensive rainfall over the Huai River basin during July 2003. Meanwhile, both diagnostic and numerical simulation studies have been performed to investigate the physical processes leading to the organization of MCSs occurring on 4–5 July 2003 (e.g., Sun et al. 2006; Wang and Ni 2006; Zhang and Zhang 2012). However, none of the previous research efforts explored the possible roles of synoptic-to-intraseasonal oscillations or waves in determining the summer 2003 heavy rainfall.

Therefore, in this study we wish to answer the following questions through spectral analysis and filtering procedures: Had any intraseasonal or synoptic-scale disturbances taken place during the summer flooding rainfall events of 2003 over YHRB? If yes, how did they contribute to the continuous and individual rainfall events? What were the structures and evolutionary patterns of these disturbances in relation to the rainfall events?

The next section describes the data and methodology used in this study. Section 3 provides a brief overview of the summer 2003 rainfall events and the associated dominant synoptic-to-intraseasonal rainfall modes over

the YHRB region. Sections 4 and 5 show the patterns of behavior and structures of the dominant synoptic-to-intraseasonal disturbances associated with the heavy rainfall events. A summary and concluding remarks are given in the final section.

2. Data and methodology

a. Data description

In this study, we use the daily rainfall data over land that were compiled by the Asian Precipitation—Highly Resolved Observational Data Integration Towards Evaluation of the Water Resources (APHRODITE) project. This dataset was constructed through the collaborative efforts of the Research Institute for Humanity and Nature and the Meteorological Research Institute of the Japan Meteorological Agency. We adopt version V0902, which includes $0.25^\circ \times 0.25^\circ$ gridded data over Asia's monsoon area and covers the period of 1961–2004. The gridded daily rainfall was obtained after interpolating rain gauge observations from meteorological and hydrological stations over the region and then performing strict quality control and objective analysis procedures (Yatagai et al. 2008, 2012).

The Interim European Centre for Medium-Range Weather Forecasts (ECMWF) Re-Analysis (ERA-Interim) (Simmons et al. 2006), which is a newly released reanalysis dataset at 1.5° resolution (http://data-portal.ecmwf.int/data/d/interim_daily/), is used herein to depict the large-scale circulation patterns associated with the summer 2003 heavy rainfall events. For our study, daily mean fields are calculated by simply averaging the original 6-hourly dataset.

b. Spectral analysis and filtering

To identify the prominent temporal range of rainfall fluctuations in the selected core region, the spectral analysis of the daily rainfall data, after removing their series means, is performed with the fast Fourier transform (FFT) method. The raw spectral estimates are smoothed and a tapered window (10% of the data) is adopted. The statistical significance of power spectra is tested, following the method of Gilman et al. (1963), which is based on the power spectrum of the mean red noise.

Periodical disturbances are extracted from the raw daily rainfall and daily mean circulation fields at each grid point through a fixed-period bandpass filtering, which is based on the Fourier harmonic analysis. The FFT is carried out for the APHRODITE daily rainfall and ERA-Interim daily mean circulation datasets throughout the

year 2003. The phase analysis method (see Fig. 3e) is used for the analyzed variables to identify the spatial structures and temporal evolution of individual disturbances. There are a total of eight phases in one life cycle. The peak dry phase (phase 1) and peak wet phase (phase 5) refer to the minimum and maximum rainfall day, respectively. Because we care mainly about how the synoptic-to-intraseasonal disturbances cause the development of heavy rainfall events, phases 1–5 will be examined in more detail in this study.

Moreover, the filtered rotational wind anomaly vectors will be used to better identify the associated lower-level disturbances at various time scales. In fact, we have also computed the column-integrated moisture flux anomaly and its divergence to identify the heavy rainfall and circulation relationship. Results indicate that these variables have similar patterns to the lower-level (850 hPa) rotational wind and surface rainfall anomalies (not shown). Therefore, we will use the bandpass-filtered rotational wind anomaly to study the relationship between surface rainfall and atmospheric circulations.

3. Overview

The warm season rainfall over east China is one of the most important indicators for the East Asian summer monsoon. From the longitudinally averaged (between 114° and 121°E) daily rainfall, as given in Fig. 1, we can see two northward migrations and three stagnations of the zonally averaged rainfall belt during summer 2003. Specifically, prior to 20 June, the rainbelt occurred mostly over south China (i.e., south of 27°N). After that date, the rainbelt exhibited a rapid northward displacement to YHRB (27° – 35°N) and was sustained until 11 July, corresponding to the traditional mei-yu season with continuous rainfall. After 11 July, the rainbelt moved to northern and northeast China (i.e., north of 35°N) with obviously decreased intensity. There was also a slight northward migration of rainfall occurring at the end of June, which might be associated with the northwestward extension of the western Pacific subtropical high (Wu and Wang 2001; Sun et al. 2004). Therefore, the mei-yu season in summer 2003 can be roughly divided into two periods: 20–29 June and 30 June–11 July.

During the first period, rainfall occurred mainly to the south of the Yangtze River (Fig. 2a), with the heaviest daily rainfall rate of 35 mm day^{-1} located at the northern region of Jiangxi Province (JX), except on 22 June when the Huai River experienced a heavy rainfall amount (Fig. 1). During the second period, the peak rainfall reached 45 mm day^{-1} , as its center moved

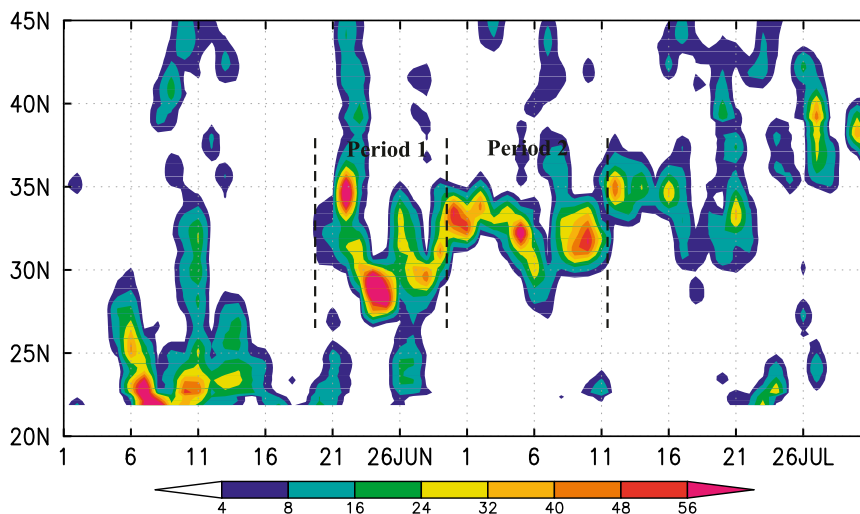


FIG. 1. Time–latitude cross section of the zonally averaged (114°–121°E) APHRODITE daily rainfall rates (mm day^{-1}) during the months of June and July 2003. The two mei-yu rainy periods [i.e., 20–29 Jun (period 1) and 30 Jun–11 Jul (period 2) 2003] are also shown.

northward to the provincial border of Anhui (AH) and Jiangsu (JS) (Fig. 2b). In contrast to the widespread rainfall over central east China during the first period, the second period was characterized by a northeast–southwest-oriented rainfall belt, with little rainfall in south China. Based on the two major rainfall periods and their

respective rainfall centers, we choose two core regions for this study (Fig. 2): southern YHRB (27°–31°N, 114°–121°E, hereafter sYHRB) and northern YHRB (31°–35°N, 114°–121°E, hereafter nYHRB), respectively.

To obtain the dominant periodicities of the rainfall intraseasonal variations over sYHRB and nYHRB,

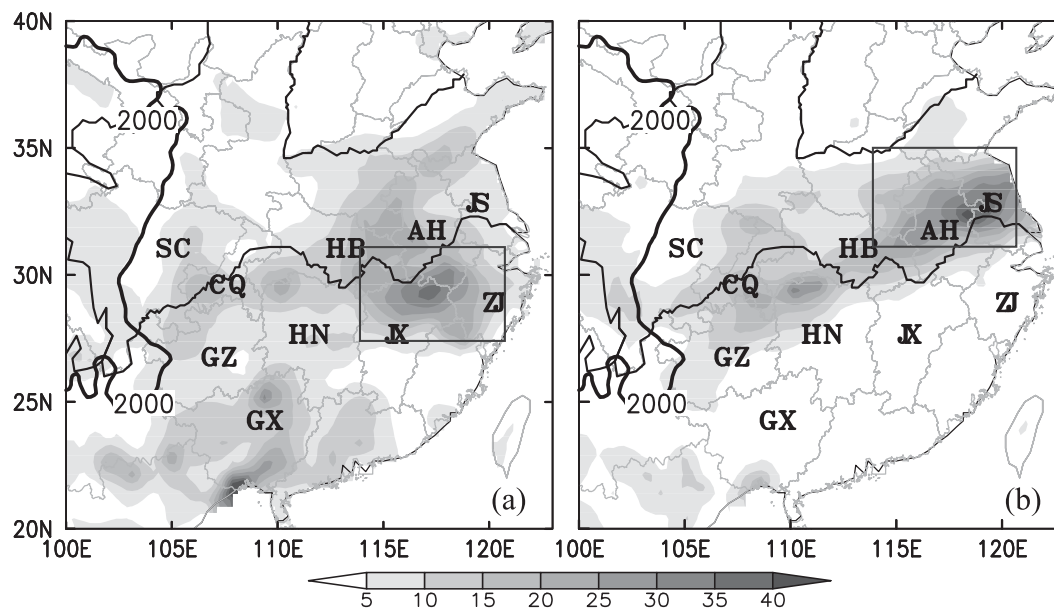


FIG. 2. Spatial distribution of the temporally averaged APHRODITE daily rainfall rates (mm day^{-1}) over east China for the periods of (a) 20–29 Jun and (b) 30 Jun–11 Jul 2003. The boxes in (a) and (b) represent the core regions of sYHRB (27°–31°N, 114°–121°E) and nYHRB (31°–35°N, 114°–121°E), respectively. Provincial boundaries (light lines), and the Yangtze and Yellow Rivers (black line) are also shown. SC, CQ, JS, GZ, YN, AH, HB, HN, JX, ZJ, and GX, denote the provinces of Sichuan, Chongqing, Jiangsu, Guizhou, Yunnan, Anhui, Hubei, Hunan, Jiangxi, Zhejiang, and Guangxi, respectively. The thick solid line denotes the distribution of 2000-m terrain elevation.

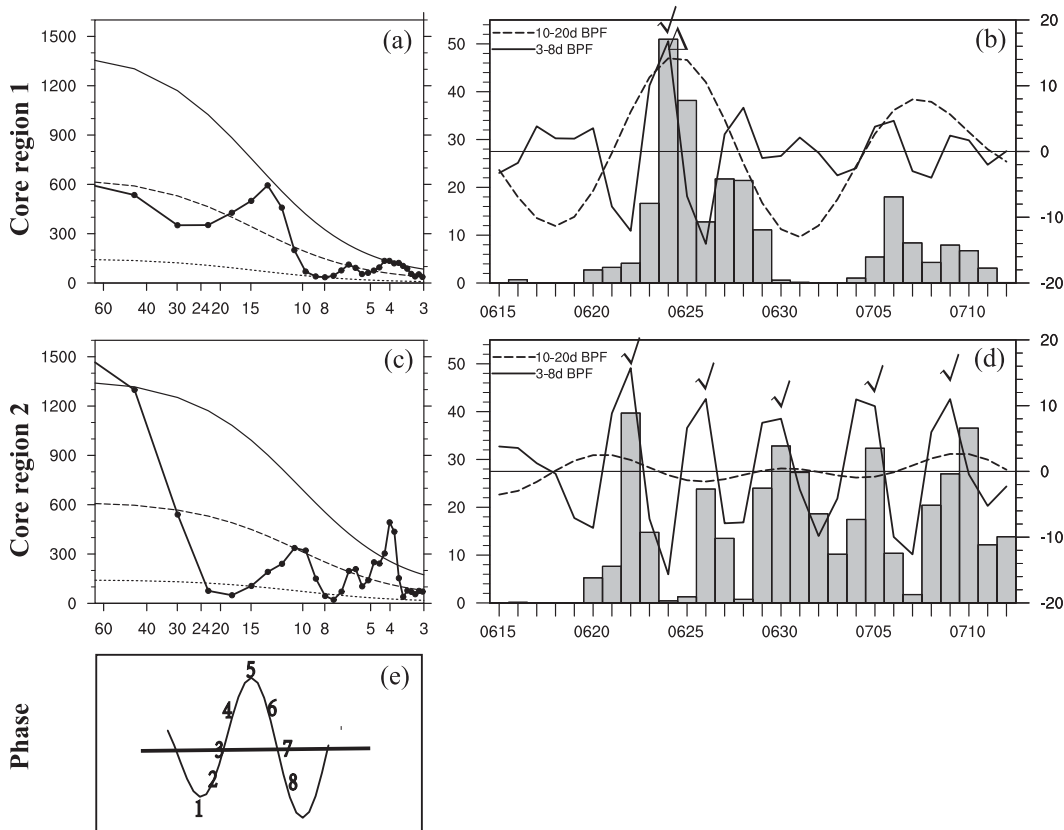


FIG. 3. (left) Power spectra of the APHRODITE daily rainfall rates over (a) sYHRB and (c) nYHRB during June–August 2003, with the calculated spectrum (solid line with dots), Markov red-noise spectrum (dashed line), and 95% upper (solid line) confidence bound. The abscissa has been rescaled to the natural logarithm of frequency. (right) Time series of the area-averaged APHRODITE daily rainfall (mm, gray bar) in the core regions of (b) sYHRB and (d) nYHRB, which is scaled on the left vertical axis, and the 10–20-day (dashed lines) and 3–8-day (solid line) bandpass-filtered daily rainfall (mm), which is scaled on the right vertical axis during the period of 15 Jun–12 Jul 2003. The triangle and tick marks denote one quasi-biweekly and six major synoptic-scale rainfall disturbances. (e) Example of eight phases in one life cycle used in the phase analysis.

Figs. 3a and 3c present the power spectra of rainfall during the months of June–August 2003 over the above-mentioned two core regions, respectively. In addition, Markov's red-noise spectrum and the 95% upper confidence bound are also shown. Two dominant frequency bands can be identified over sYHRB during the summer season of 2003 (Fig. 3a): one on days 10–20 (quasi biweekly) and the other on days 3–8 (synoptic time scale), which are both significant against the red-noise background. For nYHRB (Fig. 3c), there is only one dominant frequency band above the 95% confidence level (i.e., days 3–8, synoptic scale). A power spectral analysis of the 850-hPa relative vorticity over the two core regions also shows similar spectral patterns (not shown).

To further extract the corresponding quasi-biweekly and synoptic-scale events, Figs. 3b and 3d compare the area-averaged daily rainfall series against the 10–20- and 3–8-day bandpass-filtered rainfall over sYHRB and

nYHRB. Over sYHRB, the heaviest rainfall (larger than 25 mm day^{-1}) occurred on 24–25 June. We see one prominent quasi-biweekly case (18–30 June) and one obvious synoptic-scale case (22–26 June) over this region. The peak wet phases of both the quasi-biweekly and synoptic-scale cases exactly matched the strongest rainfall event on 24 June. The significant quasi-biweekly cycle from 18 to 30 June happened to cover the sYHRB mei-yu rainy phase, with its two dry peaks (i.e., 18 and 30 June) corresponding to days with less rainfall. Based on the area-averaged total and filtered rainfall variances, the quasi-biweekly and synoptic-scale modes show nearly equal contributions to the total rainfall, namely, 33.0% and 35.9%, respectively (Table 1). In contrast, a total of five synoptic-scale heavy rainfall events (larger than 25 mm day^{-1}), corresponding to the peak rainfall on 22, 26, and 29–30 June, and 5 and 9–10 July (see the ticks in Fig. 3d), hit nYHRB during the

TABLE 1. The total, 3–8-day, and 10–20-day bandpass-filtered rainfall variances ($\text{mm}^2 \text{day}^{-2}$) and their percentage during intensive rainfall periods over two different regions.

Time period	Region	Total rainfall variance	3–8-day filtered rainfall variance	10–20-day filtered rainfall variance
20–30 Jun 2003	sYHRB (27°–31°N, 114°–121°E)	252.33	90.55 (35.9%)	83.32 (33.0%)
20 Jun–12 Jul 2003	nYHRB (31°–35°N, 114°–121°E)	140.13	85.85 (61.3%)	1.87 (1.3%)

period of 20 June–11 July, finally leading to the severe flooding across this region. Clearly, the synoptic-scale mode made a major contribution (i.e., 61.3%) to these rainfall events (Table 1).

In the two sections that follow, the associated circulations of the quasi-biweekly rainfall case (i.e., peaked on 24 June) over sYHRB and the six synoptic-scale cases over both sYHRB and nYHRB (i.e., peaked on 24, 22, 26, and 30 June, and 5 and 9 July) will be explored in detail, respectively.

4. Filtered circulations associated with the sYHRB rainfall

To evaluate the relative contributions from the quasi-biweekly and synoptic-scale disturbances to the heavy rainfall over sYHRB, Fig. 4 shows the daily rainfall, the 850-hPa horizontal wind vectors, and the 500-hPa 5880-m geopotential isoline (Fig. 4a); as well as the 10–20-day (Fig. 4b) and 3–8-day (Fig. 4c) bandpass-filtered 850-hPa wind vectors during the peak wet phase (i.e., phase 5 on

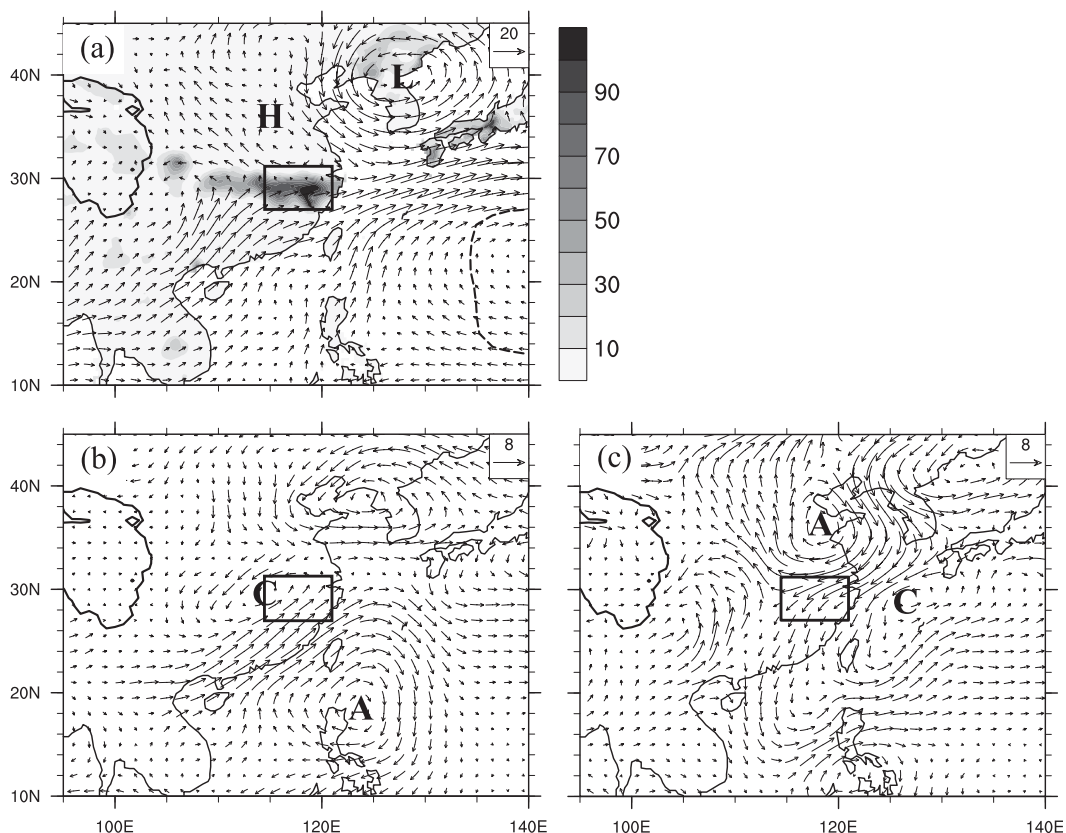


FIG. 4. (a) The 850-hPa daily mean wind vectors (m s^{-1}) and daily rainfall (shaded, mm) on 24 Jun 2003. (b) The 10–20- and (c) 3–8-day bandpass-filtered 850-hPa daily mean wind anomalies on 24 Jun 2003. Letters L, H, A, and C denote low and high pressure systems, the centers of an anticyclonic anomaly, and a cyclonic anomaly, respectively. Dashed lines in (a) refer to the 500-hPa 5880-m geopotential isoline. The box in each frame represents sYHRB (27°–31°N, 114°–121°E). The periphery of the Tibetan Plateau (>3000m) is also shown. The remaining figures follow a similar format.

24 June). We see an east–west-oriented heavy rainfall belt that coincided with a lower-level cyclonic shear line where the mei-yu front with large θ_e gradients (not shown) was located (Fig. 4a). Apparently, this rainfall belt was generated by organized convergence along the mei-yu front as the tropical warm and moist air was transported by southwesterly monsoonal flows and, then, met with a higher-latitude cold high. In the quasi-biweekly (10–20-day) filtered lower-level wind field, the presence of a cyclonic anomaly over the sYHRB region and an anticyclonic anomaly over the Philippines gave rise to the pronounced southwesterly anomalies over southeastern China (Fig. 4b).

In contrast, the synoptic-scale (3–8-day) filtered wind field exhibited quite different circulation anomalies (Fig. 4c). There was an intense anticyclonic anomaly over the Shandong Peninsula (centered over 37°N, 120°E) and a northeast–southwest-oriented cyclonic anomaly over the wide area from the East China Sea to the South China Sea. The western Pacific subtropical high exhibited a sudden eastward retreat from 23 to 24 June, as is to be expected from the emergence of the cyclonic–anticyclonic anomaly couplet. With the combined influence of the cyclonic–anticyclonic anomaly couplet, the northeasterly anomalies swept through sYHRB and southern China. However, because the southwesterly anomalies of quasi-biweekly disturbances were stronger than the northeasterly anomalies of synoptic-scale disturbances over south China, the subtropical warm and moist air was allowed to reach sYHRB at the peak wet phase, despite the fact that the western Pacific subtropical high was located farther east. Therefore, the quasi-biweekly and synoptic-scale disturbances contributed southwesterly and northeasterly anomalies to the wind shear line along sYHRB, respectively. In the following two subsections, we discuss how the associated anticyclonic anomalies or cyclonic anomalies at the two different time scales are generated.

a. Structures and evolution of the quasi-biweekly disturbance

To help us examine the circulation characteristics at the quasi-biweekly time scale, Fig. 5 shows the temporal evolution of the quasi-biweekly bandpass-filtered 850- and 200-hPa circulations, together with the corresponding rainfall and divergence anomalies from phase 1 to 5. In the lower troposphere, we see a well-defined northwest–southeast-oriented anomaly couplet at the peak wet phase, with a cyclonic anomaly over sYHRB and an anticyclonic anomaly over the Philippines (Fig. 5i). Meanwhile, a north–south-oriented anomaly couplet took place over east China in the upper troposphere,

with a cyclonic anomaly over north China and an anticyclonic anomaly over south China (Fig. 5j). A mirror image of the phase 5 features could also be seen at phase 1 when the minimum rainfall anomaly occurred over sYHRB (Figs. 5a,b).

Since the lower-level cyclonic–anticyclonic anomaly couplet was closely related to the sYHRB heavy rainfall, one may wonder where the two entities were originated at the peak wet phase. At phase 1, the anticyclonic anomaly appeared in the southeastern Philippines with the cyclonic anomaly to the northwest. From phase 2 to 3, the anticyclonic anomaly moved northwestward from 10° to 15°N along the longitudes between 120° and 130°E, while the cyclonic anomaly diminished as it went northeastward (Figs. 5c,e). With the further northwestward migration of the anticyclonic anomaly over the Philippines, its southwesterly anomalies began to influence the southeastern coast of China at phase 4 (Fig. 5g) and prevailed at phase 5 (Fig. 5i). The strong southwesterly anomalies tended to transport large amounts of moisture from the South China Sea to sYHRB, providing the needed moisture supply for the heavy rainfall. This is reflected by a positive rainfall anomaly in east China and rapid intensification of a positive specific humidity anomaly over sYHRB from phase 4 to 5 (not shown). The formation and its subsequent northwestward migration of the anticyclonic anomaly at the quasi-biweekly time scale have been extensively studied (e.g., Chen and Sui 2010; Yang et al. 2010). The anticyclonic anomaly has been found to emerge from the equatorial region, originating from equatorial Rossby waves (Chen and Sui 2010).

As the anticyclonic anomaly moved northwestward at phase 3, a new lower-level cyclonic anomaly started developing in association with a positive rainfall anomaly over Sichuan Basin (Figs. 5e,g). This cyclonic anomaly grew rapidly as it moved southeastward in east China until phase 5. This cyclonic anomaly was the key disturbance associated with the maximum positive rainfall anomaly at phase 5. An important question one may ask is: What mechanism(s) plays a role in the cyclonic anomaly's formation? We try to address this question from the following three avenues. First, the anticyclonic anomaly over the Korean Peninsula was a quasi-barotropic system, which propagated eastward as a result of the upper-level steering flow (cf. Figs. 5a and 5b). Its intensity weakened from phase 1 to 3, as did its associated southwesterly anomalies (Figs. 5c,e). Regardless of the anticyclonic anomaly evolution to the north, the southwesterly anomalies associated with the summer monsoon were maintained to the east of the Tibetan Plateau and exhibited increasing cyclonic circulations and positive rainfall anomalies over the eastern Sichuan Basin (near

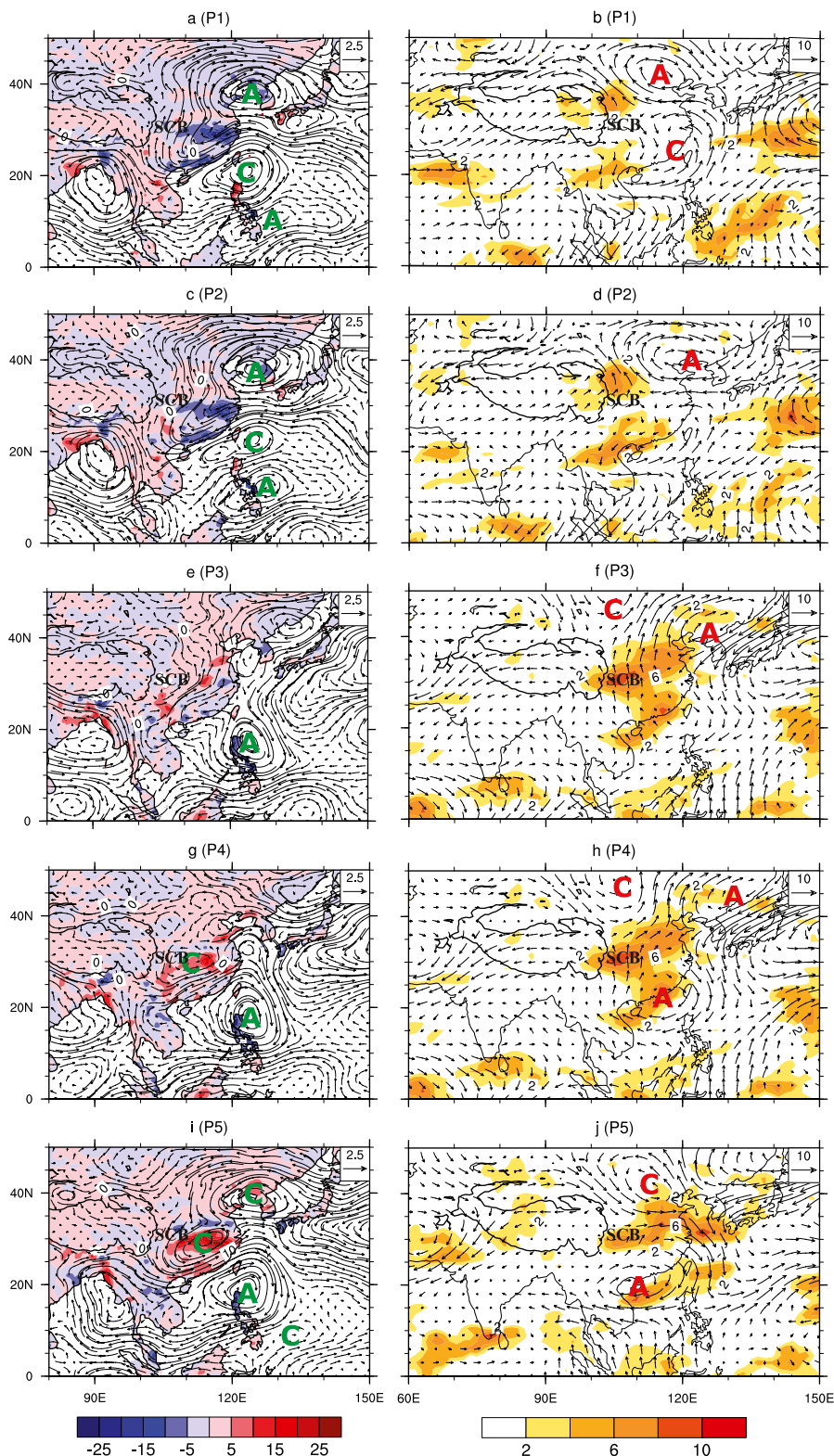


FIG. 5. Temporal evolution of (left) the 10–20-day bandpass-filtered 850-hPa daily mean rotational wind vectors (m s^{-1}) and daily rainfall anomalies (shaded, mm day^{-1}) and (right) the 10–20-day bandpass-filtered 200-hPa daily mean wind vectors (m s^{-1}) and divergence (shaded, $1 \times 10^{-6} \text{ s}^{-1}$) from phase 1 (P1, 18 Jun) to phase 5 (P5, 24 Jun). SCB denotes the Sichuan Basin.

30°N, 112°E) at phase 3 (Fig. 5e). In fact, we can see divergence aloft over northeastern Tibetan Plateau beginning in phase 1 (Fig. 5b), and it was strengthened at phase 2 (Fig. 5d). This upper-level divergence is quasigeostrophically related ahead of the upper-level trough axis. Therefore, quasigeostrophic ascent in the lower troposphere should be expected at phase 2 by the mass continuity. This would facilitate the lower-level convergence, latent heat release, and the generation of cyclonic vorticity to the east of the Tibetan Plateau.

Second, the presence of the anticyclonic anomaly over the Philippines greatly strengthened the southwesterly anomalies, with abundant moisture supply in the lower troposphere from phase 3 to 4 over south China (Figs. 5e,g). Consequently, a positive feedback process was established between the upper-level divergence, upward motion, latent heat release, and surface pressure falls. This positive feedback would facilitate the formation of a lower-level cyclonic anomaly and an upper-level anticyclonic anomaly with well-organized circulations over southern China at phase 4 (Figs. 5g,h). These disturbances reached their maximum strengths at phase 5 (Figs. 5i,j). Last and perhaps more importantly, the existence of the Tibetan Plateau also favored the development of a cyclonic circulation pattern over the Sichuan Basin, which has been often called the southwest vortex. It has been considered as being topographically forced, as the southwestern Asian monsoonal flow climbs and cyclonically turns around the southeast corner of the Tibetan Plateau (Zhu et al. 2000). Some southwest vortices may also originate from the eastward propagation of mesolows over the Tibetan Plateau (Yasunari and Miwa 2006; Fujinami and Yasunari 2009).

It is evident that at the quasi-biweekly time scale that the upper and lower parts of the troposphere were fully coupled through upward motion and latent heat release associated with the heavy rainfall. Due to the importance of moisture transport, the lower-level disturbances played key roles in determining the intensity of rainfall in sYHRB. When the subtropical anticyclonic anomaly and midlatitude cyclonic anomaly were phase locked, the sYHRB rainfall reached its peak wet phase. It appears to be the large-scale background flows that determined the quasi-biweekly activity only over sYHRB in 2003. That is, on 18–24 June, under the influence of the southeasterly (southwesterly) from the western Pacific subtropical high that was still over the northwestern Pacific (not shown), the anticyclonic (cyclonic) anomaly over the northwest Philippines (YRB) could not propagate farther northwestward (northeastward) into the nYHRB region.

b. Structures and evolution of the synoptic-scale disturbance

In the upper troposphere, the most obvious feature at the synoptic scale was the propagation of alternating anticyclonic and cyclonic anomalies zonally along 40°N latitude (see the right panel in Fig. 6). These disturbances were typically organized in a baroclinic Rossby wave train, which was characterized by a zonal planetary wavenumber of about 9 with a phase speed of about 9.5 ms^{-1} . But these disturbances propagated eastward with phase speeds greater than those typical of synoptic systems over other continents, such as African easterly waves and monsoon lows over the Indian subcontinent (Berry et al. 2012), because of the influence of background westerly jet streams aloft. The existence of the upper-level Rossby waves helped the lower-level midlatitude synoptic-scale disturbances propagate northeastward (or eastward) (see the left panel in Fig. 6).

In contrast, the lower-tropospheric disturbances were not as regular as their upper-level counterparts (Fig. 6). Given that, one still can see the periodic generation of anticyclonic and cyclonic anomalies on the downstream side of the Tibetan Plateau and the subsequent northeastward displacement through advection by background monsoonal flows plus the upper-level steering effects. These disturbances tended to intensify as a result of vortex stretching associated with rainfall anomalies as they moved northeastward across the YHRB region into higher latitudes. Specifically, the cyclonic anomaly over the Philippines went northeastward from phase 1 to 3 (Figs. 6a,c). As it moved toward the East China Sea at the peak wet phase, the northeasterly anomalies were enhanced and precipitation over south China was suppressed. Its northeastward displacement also made the western Pacific subtropical high retreat farther eastward (Fig. 4a). Meanwhile, two weak anticyclonic anomalies, one over the South China Sea and the other to the southeast of the Tibetan Plateau, merged over the YHRB region, and at phase 5, it merged with the anticyclonic anomaly previously located to the north of 40°N, forming an intense anticyclonic anomaly centered near 35°N, 120°E (Fig. 6e). The development of this anticyclonic anomaly allowed higher-latitude cold and dry air to intrude into sYHRB. As the anticyclonic anomaly to the southeast of the Tibetan Plateau moved toward the YHRB region, a new cyclonic anomaly with a positive rainfall anomaly formed locally at the same position as the anticyclonic anomaly (Fig. 6e). This cyclonic anomaly appeared to play an important role in generating the heavy rainfall over nYHRB on 26 June (see section 5).

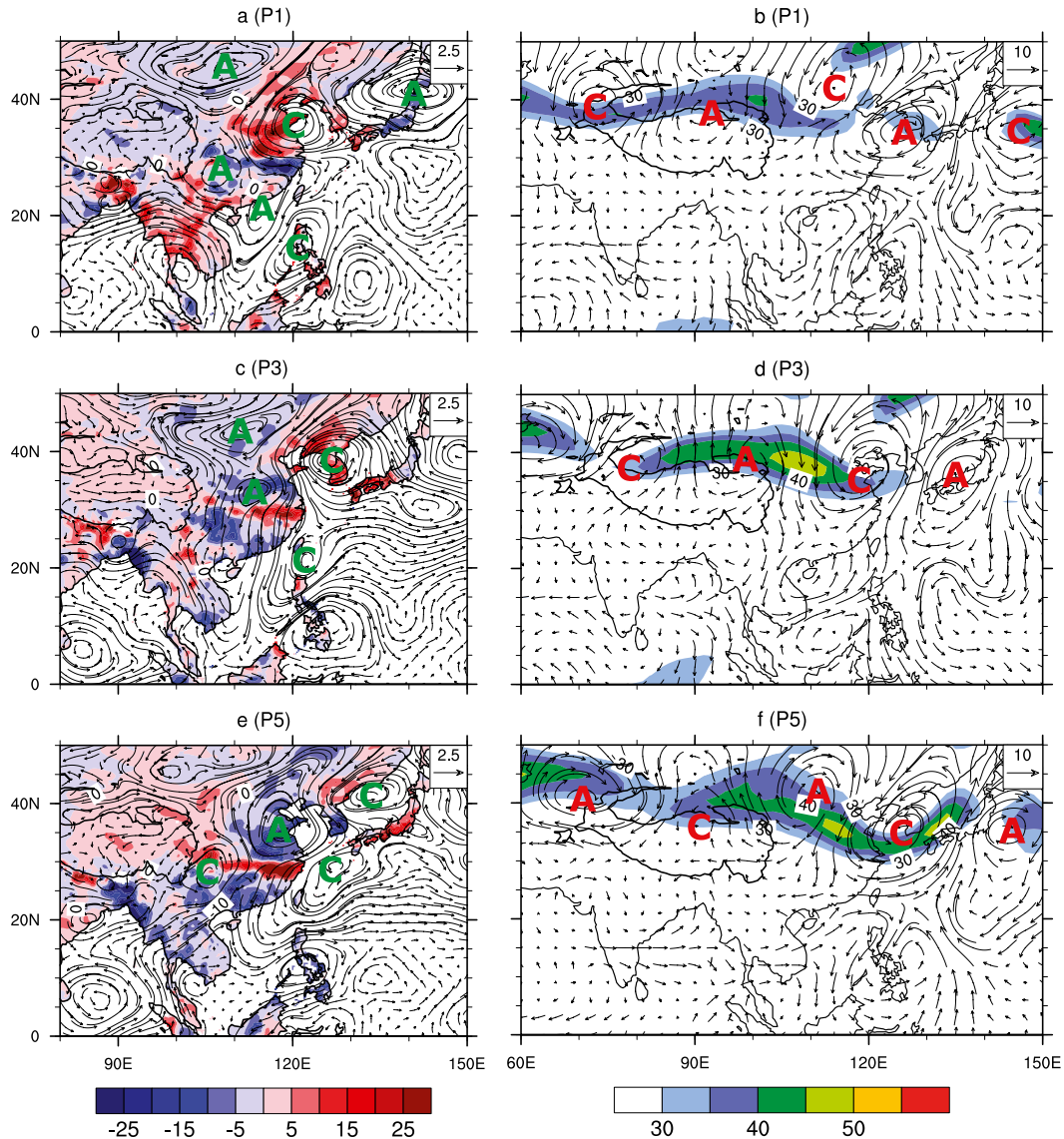


FIG. 6. Temporal evolution of (a),(c),(e) the 3–8-day bandpass-filtered 850-hPa daily mean rotational wind vectors (m s^{-1}) and daily rainfall (shaded, mm) and (b),(d),(f) the 3–8-day bandpass-filtered 200-hPa daily mean wind vectors (m s^{-1}) and the corresponding total wind speed (shaded) [on 22 (P1), 23 (P3), and 24 (P5) Jun 2003]. Wind speeds above 30 m s^{-1} are shown at intervals of 5 m s^{-1} .

Another different phenomenon between the synoptic-scale disturbances and the quasi-biweekly variation is that sYHRB was under the complete control of cold and dry anomalies throughout the troposphere after phase 2, with the peak intensity at phase 5 (Fig. 7). Evidently, it was the northeasterly to northerly anomalies in the deep troposphere that transported the cold and dry air masses from higher latitudes to south China. This precipitation process is similar to the continuous rainfall events over YHRB during the first mei-yu period of summer 1998, during which midlatitude disturbances interacting with cold and dry air from higher latitudes

accounted for the development of the flooding rainfall (Liu et al. 2008).

5. Filtered circulations associated with the nYHRB rainfall

Because we focus more on the disturbances at the synoptic and longer time scales in this study, MCSs are considered to be “transient” systems and could not be examined from the daily mean fields, although they were the agents of heavy rainfall production. Figures 8a–e show the daily mean large-scale flow patterns associated

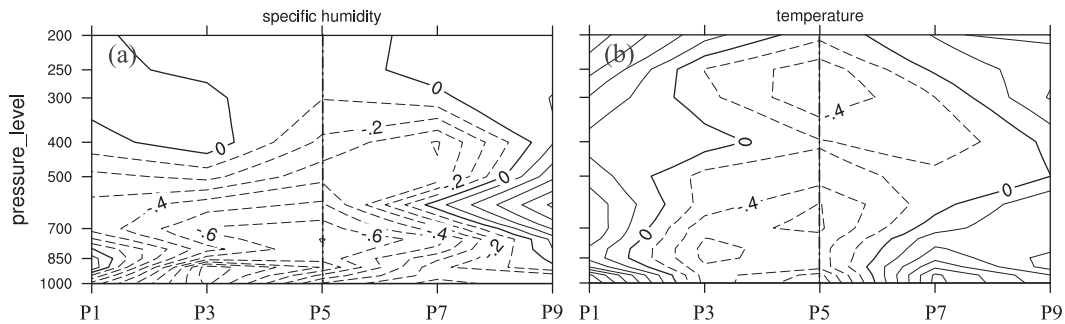


FIG. 7. Phase–pressure diagrams of the 3–8-day bandpass-filtered sYHRB area-averaged (a) specific humidity (g kg^{-1}) and (b) temperature ($^{\circ}\text{C}$). The vertical dash-dot lines refer to the peak wet phase (phase 5) on 24 Jun 2003.

with the five nYHRB rainfall events on the heaviest rainfall days, respectively. It is evident that among the five nYHRB rainfall events, three of them (i.e., 22 and 26 June, and 5 July) were caused by the low pressure systems moving along the mei-yu front (Figs. 8a,b,d), and the other two (i.e., 30 June and 9 July) resulted from the mei-yu front (Figs. 8c,e). As we will see later, the mid- to high-latitude anticyclonic anomalies played an important role in triggering the mei-yu frontal rainfall for the last two rainfall events (Figs. 11e and 13e), as well as the previously analyzed 24 June sYHRB rainfall event (Fig. 6e). Among the five rainfall cases, except for the 26 June rainfall event, southeastern China was dominated mostly by the western Pacific subtropical high. The southwesterly winds along the western edge of the western Pacific subtropical high ensured the persistent moisture supply from the South China Sea to nYHRB.

Figures 9–13 present the filtered synoptic-scale disturbances in both the lower and upper troposphere associated with the five nYHRB intensive rainfall events, respectively. It appears that the peak rainfall over nYHRB on 22 June was directly caused by a cyclonic anomaly located over Shandong Peninsula, which had its origins over south China during phase 1 (cf. Figs. 9a and 9e). From phase 1 to 3, the easterly anomalies of an anticyclonic anomaly near the Korean Peninsula helped transport moisture from the East China Sea to nYHRB, facilitating the development of heavy rainfall (Figs. 9a,c). The associated latent heating in turn enhanced the cyclonic anomaly over nYHRB. Meanwhile, a Rossby wave train propagated northwestward across the Philippines from the tropics to south China, with an isolated anticyclonic anomaly over the South China Sea at phase 5 (Fig. 9e). The northwestward movement of this anticyclonic anomaly shifted the western Pacific subtropical high to south China. Hence, the background southwesterly winds associated with the western Pacific subtropical high provided necessary moisture supply

to nYHRB on the peak wet day (Fig. 8a). In the upper troposphere, an anticyclonic anomaly was located right over nYHRB from phase 3 to 5 (Figs. 9d,f). This baroclinic vertical structure intensified the local upward motion and maximized the positive rainfall anomaly over nYHRB.

A northeastward-propagating wave train from downstream of the Tibetan Plateau to the Sea of Japan was apparent from phase 1 to 5 for the 26 June rainfall event (Figs. 10a,c,e). The heavy rainfall on phase 5 also coincided with the development of a cyclonic anomaly over nYHRB. The cyclonic anomaly first appeared to the east of the Tibetan Plateau at phase 1, and it was then strengthened as it went northeastward with a positive rainfall anomaly. The southerly anomalies of the anticyclonic anomaly, located over the northeastern Philippines, provided necessary moisture from the subtropical ocean to nYHRB at phase 5 (Fig. 10e). In the upper troposphere, the Rossby wave trains were almost restricted within 35° – 45°N (see the right panel in Fig. 10). This tended to limit the meridional exchange of heat and momentum between baroclinic eddies.

The 28–30 June rainfall event was more related to the mei-yu front, like the 24 June sYHRB heavy rainfall (cf. Figs. 4a and 8c). In the lower troposphere, the southwesterly anomalies associated with a cyclonic anomaly over central China transported needed moisture to the mei-yu front at phase 3 (Fig. 11c). Meanwhile, nYHRB was situated at the right entrance region of an upper-level jet stream during phase 3–5 (Figs. 11d,f), which was a favorable region for upward motion. However, strong lower-level easterly anomalies dominated nYHRB on the peak wet day (Fig. 11e). Figure 14 shows the presence of much more intense cold and dry air anomalies than those associated with the previous two rainfall events, which was consistent with the development of an intense anticyclonic anomaly to the north of nYHRB. The strong easterly flows into nYHRB was also reinforced by a cyclonic anomaly located to the east of

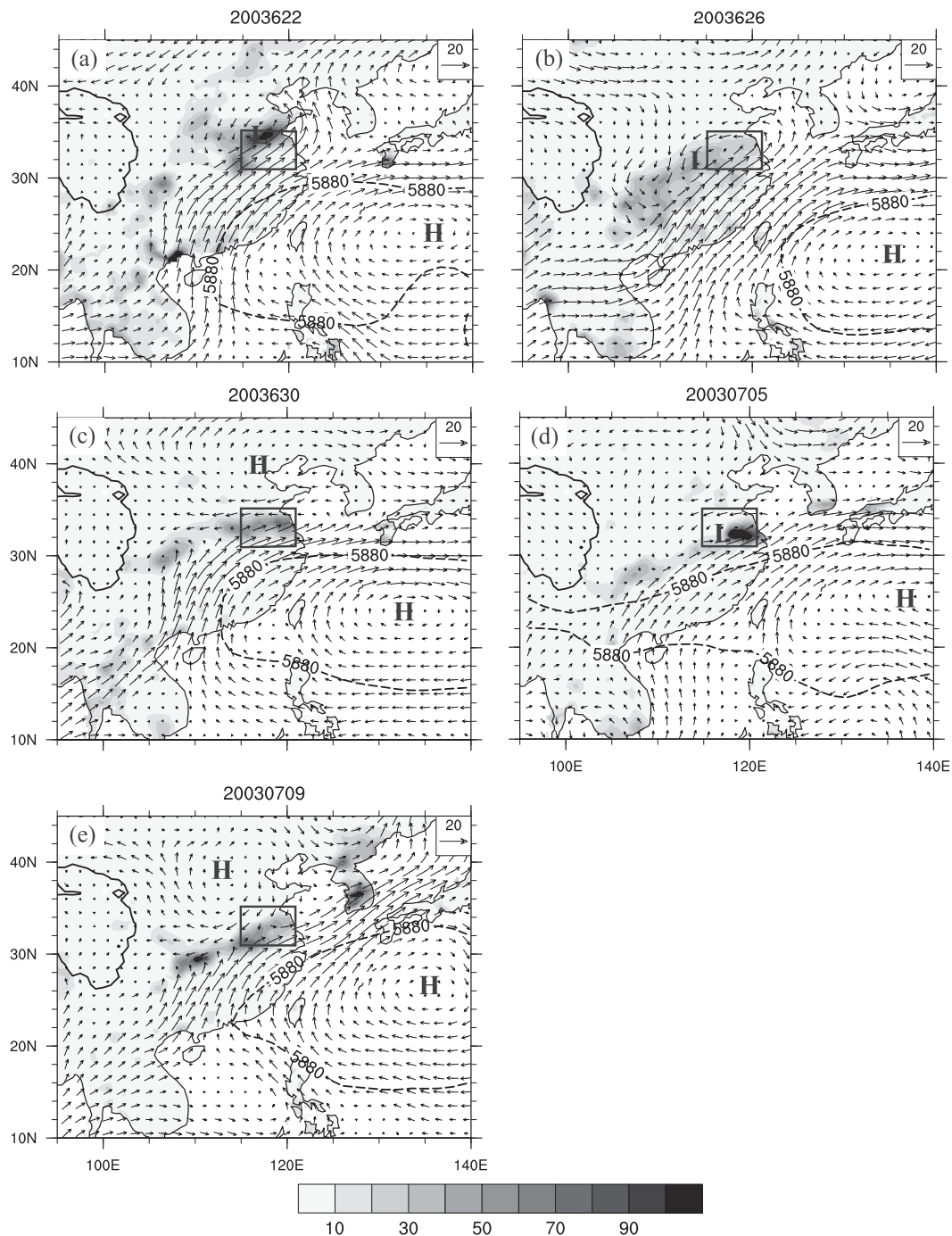


FIG. 8. The 850-hPa daily mean wind vectors (m s^{-1}) and daily rainfall (shaded, mm) on (a) 22 Jun, (b) 26 Jun, (c) 30 Jun, (d) 5 Jul, and (e) 9 Jul 2003. Dashed lines refer to the 500-hPa 5880-m geopotential isoline. The box in each frame represents nYHRB (31° – 35° N, 114° – 121° E).

Taiwan, which is similar to the flow anomaly patterns on 24 June (cf. Figs. 11e and 6e).

During the period of 3–5 July, two slowly moving baroclinic Rossby wave trains with opposite displacements appeared in the upper troposphere, one along

40°N and the other along 20°N (see the right panel in Fig. 12). As one eastward-propagating cyclonic anomaly moved to the same longitude as the northwestward-propagating cyclonic anomaly at phase 5, the two cyclonic anomalies became coupled meridionally (Fig. 12f).

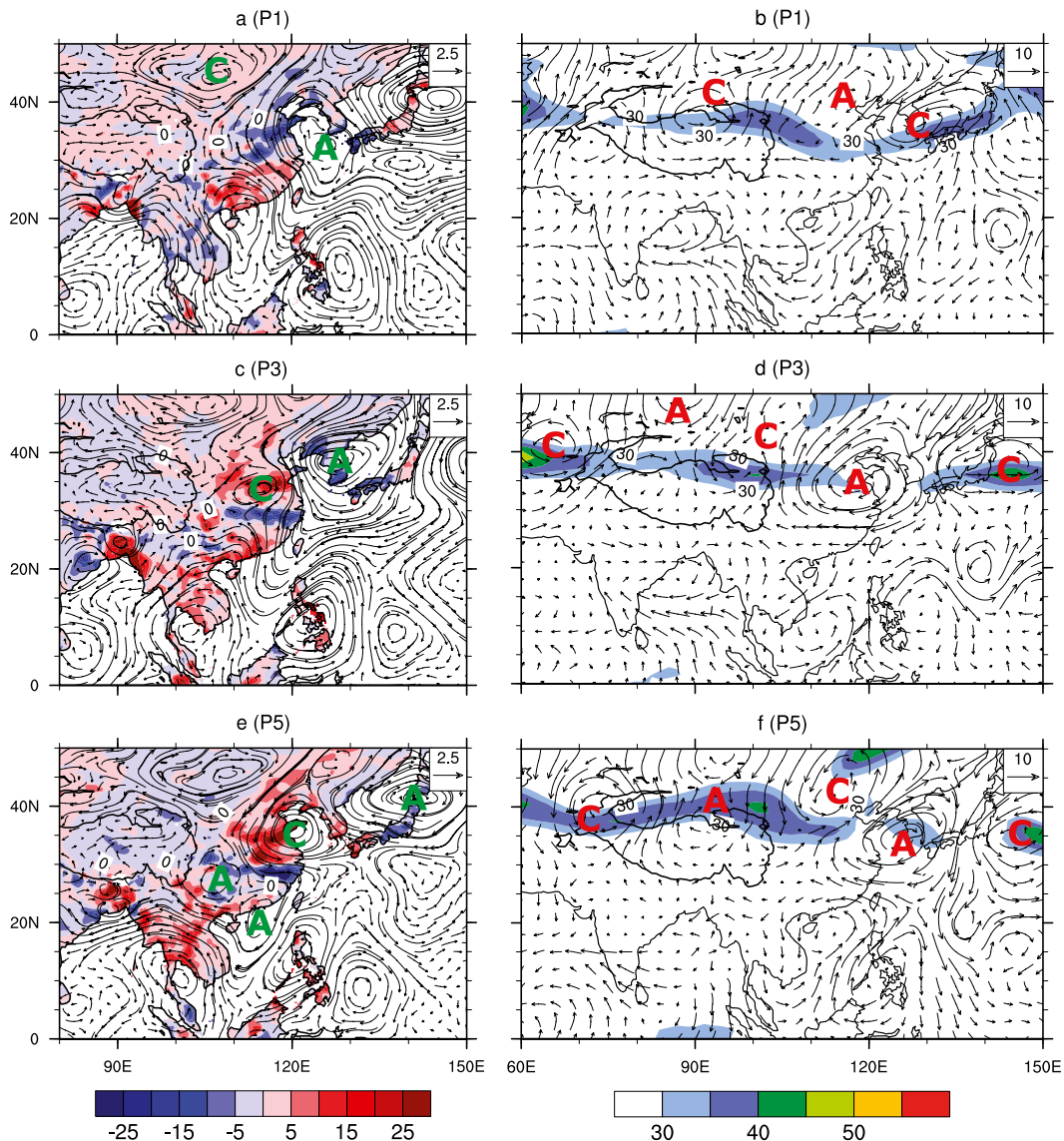


FIG. 9. As in Fig. 6, but for the synoptic-scale disturbances on 20 (P1), 21 (P3), and 22 (P5) Jun 2003.

Again, nYHRB was situated at the right entrance region of an upper-level jet stream during phases 3–5. Similarly, a lower-tropospheric Rossby wave train moved westward in the lower latitudes; they were nearly barotropically coupled with their upper-level counterparts. Meanwhile, a small and weak couplet of anticyclonic–cyclonic anomalies propagated eastward from the foothills of the Tibetan Plateau toward nYHRB (Figs. 12a,c,e), with an anticyclonic anomaly in both the lower and higher latitudes. At phase 5, the cyclonic anomaly over nYHRB was situated between the two meridionally coupled cyclonic anomalies in the upper level, but sandwiched by the two lower-level anticyclonic anomalies (Figs. 12e,f). The upper-level

flow anomalies and the jet stream structure favored the generation of quasigeostrophic upward motion over the nYHRB region, whereas the lower-level anomalies helped transport moisture into nYHRB. In addition, the anticyclonic anomaly in higher latitudes tended to enhance the cyclonic shear, which in turn at least favored the maintenance of the cyclonic anomaly over nYHRB (Fig. 12e).

A lower-tropospheric Rossby wave train could also be seen in the fifth rainfall event on 9 July (Figs. 13a,c,e). However, the flow anomaly patterns in the upper troposphere were not as regular as those shown in Figs. 9–12, with little evidence of a waveguide (Figs. 13b,d,f). It is apparent from Fig. 13 that the positive rainfall anomalies

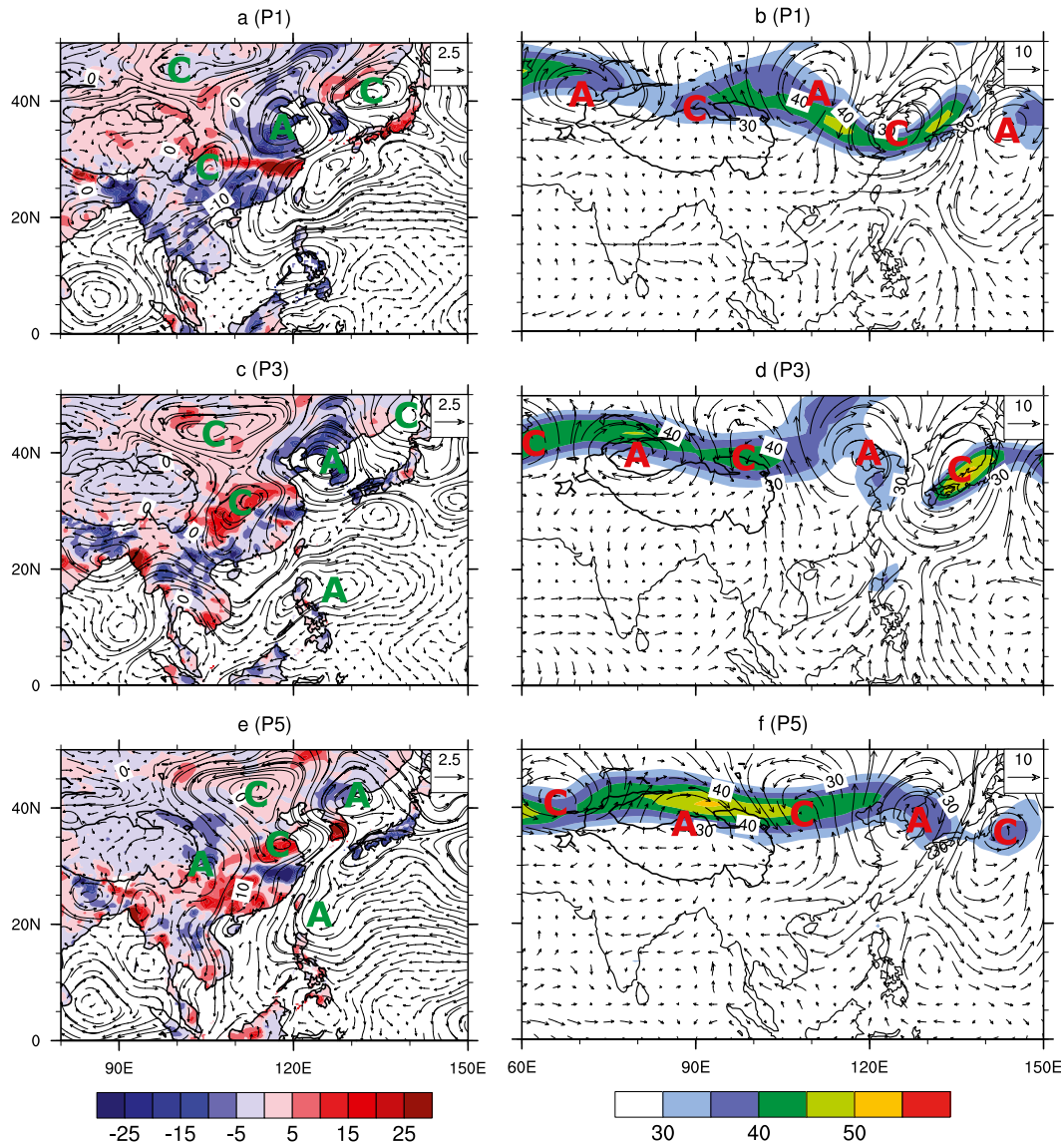


FIG. 10. As in Fig. 6, but for the synoptic-scale disturbances on 24 (P1), 25 (P3), and 26 (P5) Jun 2003.

were always associated with cyclonic circulation anomalies over nYHRB, albeit in an elongated narrow zone during the peak wet phase (Fig. 13e). During phase 5, heavy rainfall occurred as an anticyclonic anomaly over north China propagated southeastward and its associated northeasterly anomalies facilitated the lifting of the warm and moist air in the background southwesterly winds. These features can be clearly seen from Fig. 14, which shows the presence of cold and dry anomalies below warm and moist anomalies.

The above-mentioned five cases of synoptic-scale disturbances have common features that indicate these disturbances originated from the periodical generations of anticyclonic and cyclonic anomalies downstream of

the Tibetan Plateau. They showed consistent northeastward displacements under the influence of the background monsoonal flows and their interactions with the higher-latitude eastward-propagating baroclinic Rossby wave trains. Their composite analysis shows similar results (not shown). These characteristics are also similar to those associated with the 24 June heavy rainfall event taking place over sYHRB.

6. Summary and concluding remarks

In this study, we investigated the development of the summer 2003 heavy rainfall over YHRB from the perspective of high-frequency disturbances. Based on the

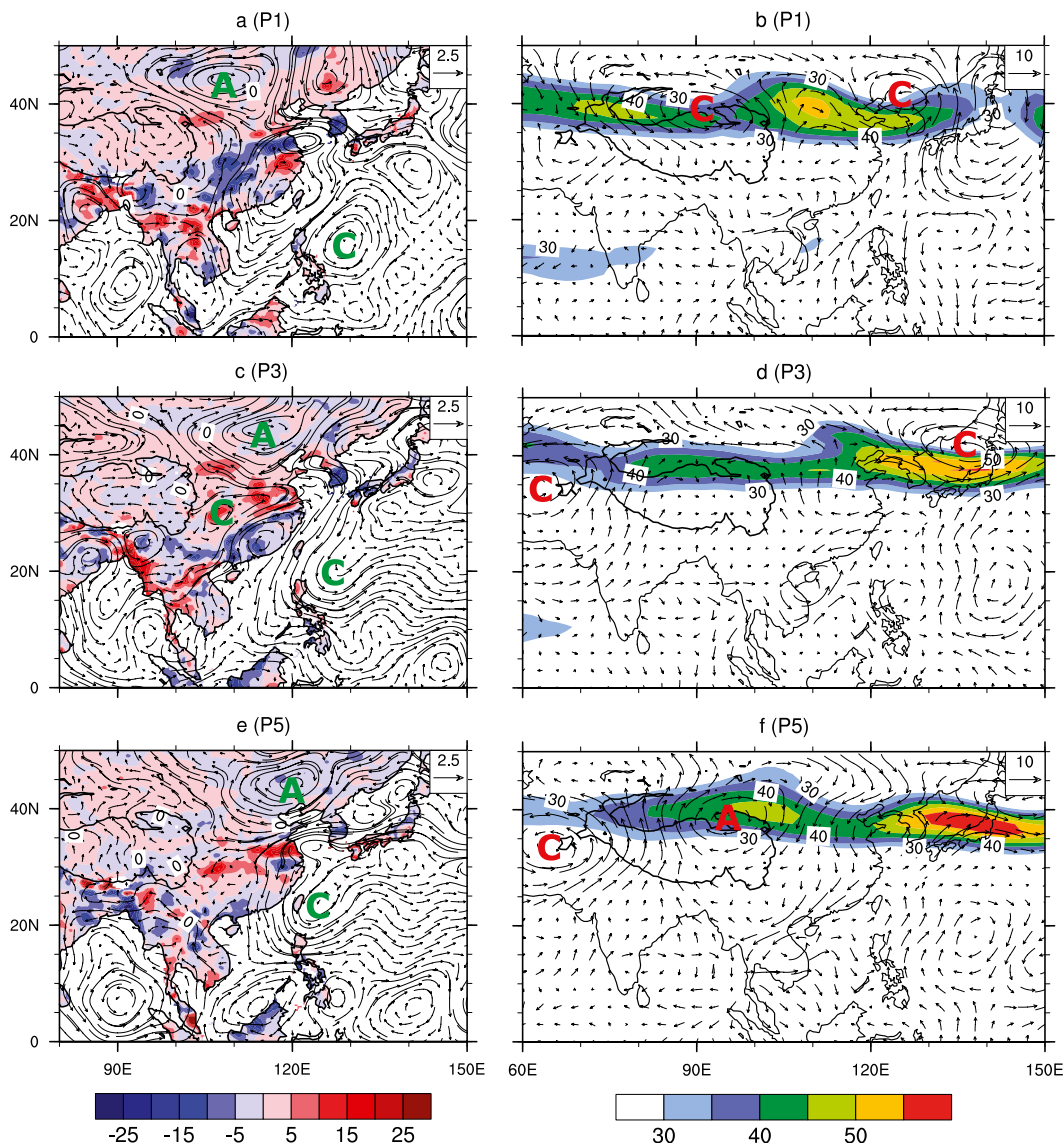


FIG. 11. As in Fig. 6, but for the synoptic-scale disturbances on 28 (P1), 29 (P3), and 30 (P5) Jun 2003.

two major rainfall periods and their respective rainfall centers, we selected two core regions, sYHRB and nYHRB, to analyze the relative roles of different disturbances in generating the heavy rainfall over these two areas. Two dominant rainfall frequency modes are identified from the spectral analysis of high-resolution daily rainfall data: one spectral peak occurring on day 14 (10–20-day variation or a quasi-biweekly mode) and the other on day 4 (3–8-day variation or a synoptic-scale mode). Results show that the sYHRB heavy rainfall event occurring on 24 June resulted from the superposition of a quasi-biweekly and a synoptic-scale disturbance, whereas the nYHRB heavy rainfall events were dominated by five respective synoptic-scale disturbances.

This is consistent with the long-lasting (short lived) nature of the sYHRB (nYHRB) rainfall events during summer 2003.

A variance analysis of the two modes shows that the quasi-biweekly and synoptic-scale disturbances played a nearly equal role in determining the sYHRB heavy rainfall on 24 June. Bandpass-filtered circulation patterns indicate that the quasi-biweekly and synoptic-scale disturbances contributed southwesterly and northeasterly anomalies, respectively, to the mei-yu frontal convergence over sYHRB at the peak wet phase. Results show that the lower and upper regions of the troposphere were fully coupled at the quasi-biweekly time scale, and the midlatitude and subtropical disturbances

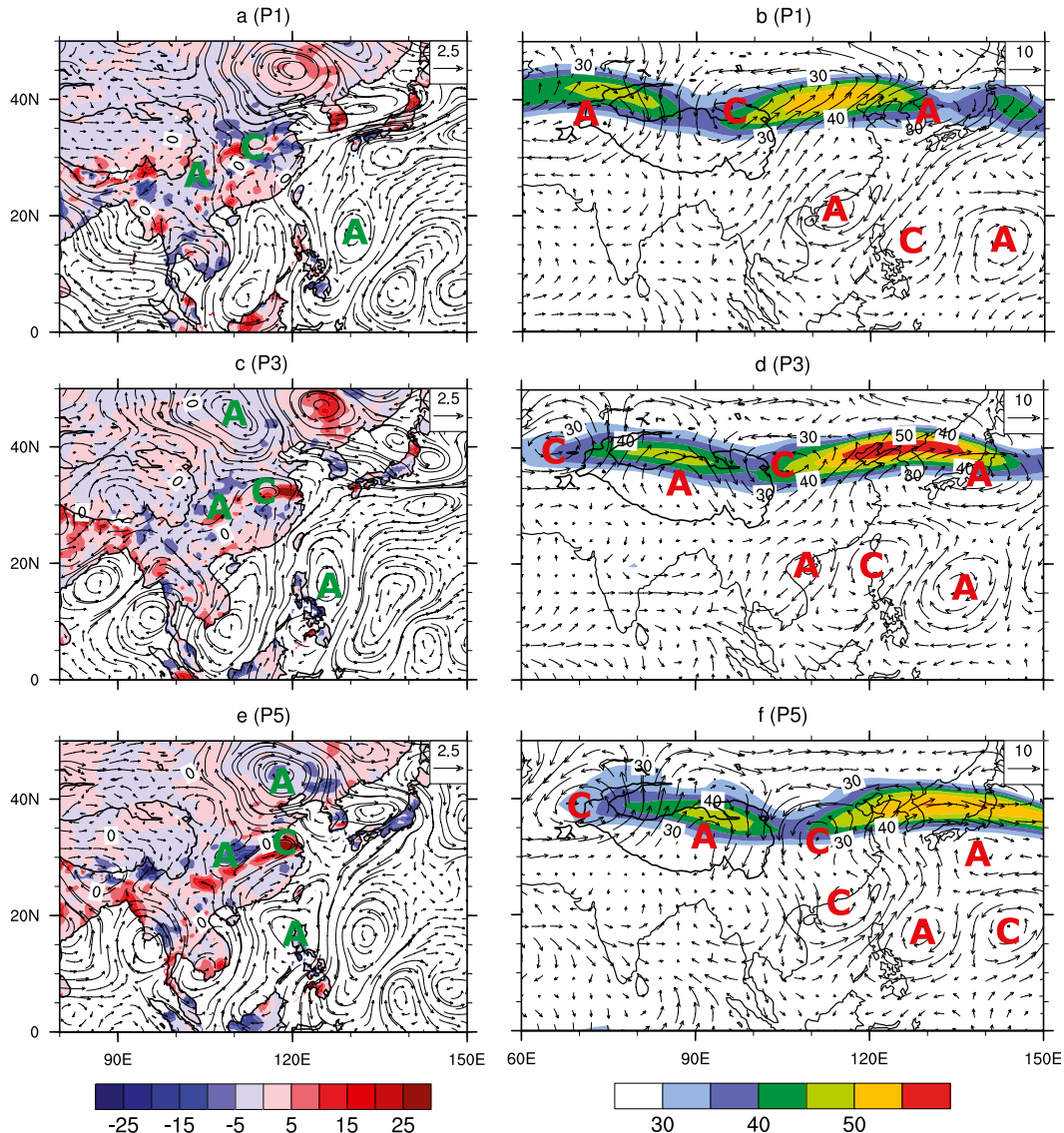


FIG. 12. As in Fig. 6, but for the synoptic-scale disturbances on 3 (P1), 4 (P3), and 5 (P5) Jul 2003.

were phase locked with a cyclonic anomaly over sYHRB and an anticyclonic anomaly over the Philippines in the lower troposphere. The cyclonic–anticyclonic anomaly couplet reached its peak intensity at phase 5, causing the maximum rainfall over sYHRB. At the synoptic scale, the strong northerly-to-northeasterly components of an anticyclonic anomaly with a deep layer of cold and dry air helped generate the sYHRB heavy rainfall.

By comparison, the flooding rainfall over nYHRB resulted from the intermittent passages of five synoptic-scale disturbances. Like the sYHRB rainfall, these disturbances were originated from the periodical generations of anticyclonic and cyclonic anomalies downstream of the Tibetan Plateau, and then displaced northeastward

under the influence of the background monsoonal flows and their interactions with higher-latitude eastward-propagating baroclinic Rossby wave trains. The lower-level cyclonic circulation anomalies coincided well with the positive rainfall anomalies on peak wet days. In addition, the subtropical disturbances provided the needed moisture supply or reinforced the northeasterly anomalies for the generation of the peak rainfall over the YHRB region. Our results suggest that synoptic-scale disturbances at higher-latitude (e.g., Rossby wave trains), midlatitude (e.g., cyclonic and anticyclonic anomalies downstream of the Tibetan Plateau), and subtropical (i.e., northwestern Pacific) regions should all be considered in order to provide properly operational

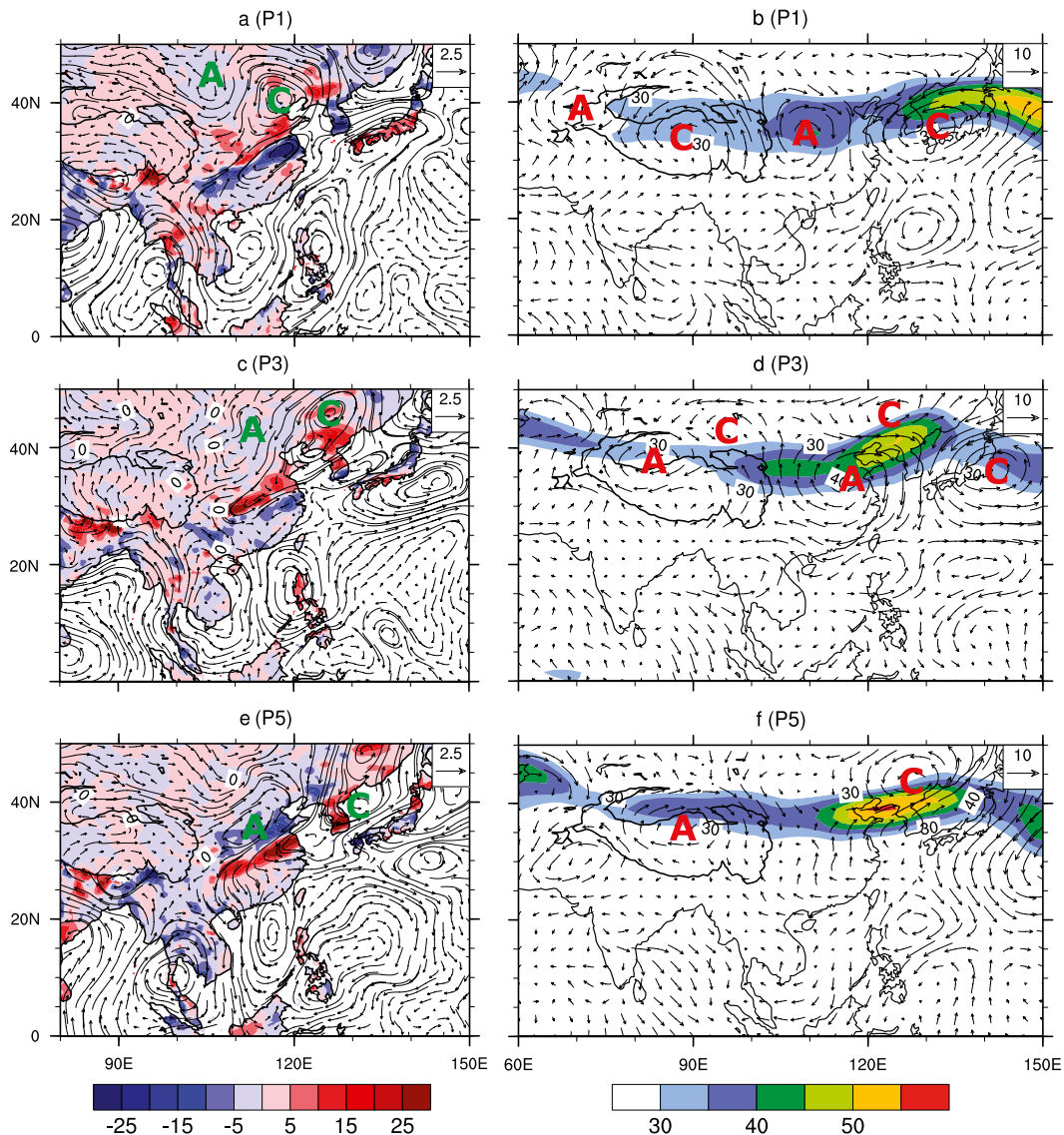


FIG. 13. As in Fig. 6, but for the synoptic-scale disturbances on 7 (P1), 8 (P3), and 9 (P5) Jul 2003.

heavy rainfall forecast guidance over the YHRB region during the mei-yu season.

It should be mentioned that many case studies of the persistent heavy mei-yu rainfall events over YHRB have been previously carried out within the context of intra-seasonal variations, but little attention has been paid to the roles of high-frequency synoptic-scale disturbances. Our study is the first to show the importance of the synoptic-scale disturbance in generating heavy rainfall events over this region. To see how robust our results are, we have applied the same analysis procedures as described in this study to the five most severe flooding rainfall events (i.e., 1991, 1998, 2003, 2005, and 2007) over YHRB during the past 20 yr, and found that the

synoptic-scale disturbances in 2003 exhibited the largest contributions (61.3%). They were also important contributors to the heavy rainfall events during the two recent flooding rainfall years of 2005 and 2007 (45.1% and 41.6%). These results support the findings presented in this study.

Clearly, our understanding of the relationship between high-frequency disturbances and the YHRB rainfall is far from complete. Further studies are needed to gain insights into what conditions favor the intermittent passage of synoptic-scale disturbances. Moreover, it is desirable to study more heavy rainfall cases over YHRB during different mei-yu seasons, in order to develop a synoptic-scale climatology, including

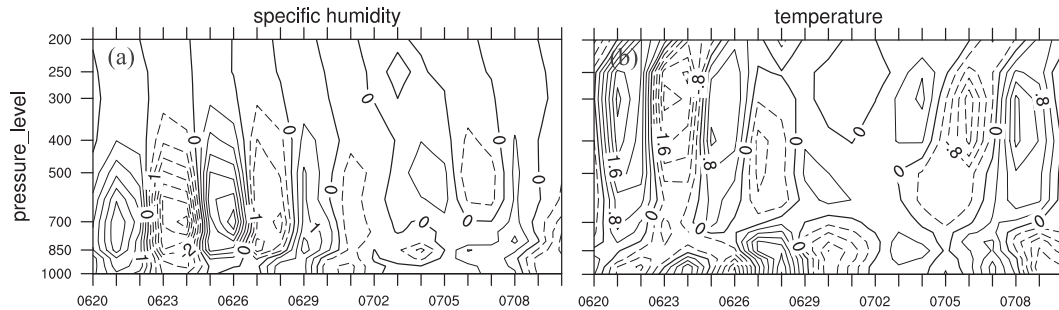


FIG. 14. Time–pressure diagrams of the 3–8-day bandpass-filtered nYHRB area-averaged (a) specific humidity (g kg^{-1}) and (b) temperature ($^{\circ}\text{C}$) during the period of 20 Jun–10 Jul 2003.

different types of synoptic-scale disturbances, to facilitate the empirical forecasting of persistent rainfall in east China during the mei-yu season.

Acknowledgments. We wish to thank two anonymous reviewers for their constructive comments. This work is jointly supported by the National Basic Research Program of China (973 Program, Grant 2012CB955401 and 2012CB417203), the National Natural Science Foundation of China (Grants 40905049 and 41375003), the China Meteorological Administration for the R&D Special Fund for Public Welfare Industry (Meteorology) (Grants GYHY201306016 and GYHY200906020), and the National High Technology Research and Development Program of China (863 Program, Grant 2010AA012304). ERA-Interim and APHRODITE data used in this study have been provided through the ECMWF (http://data-portal.ecmwf.int/data/d/interim_daily/) and APHRODITE's water resources project (<http://www.chikyu.ac.jp/precip>).

REFERENCES

- Berry, G. J., M. J. Reeder, and C. Jakob, 2012: Coherent synoptic disturbances in the Australian monsoon. *J. Climate*, **25**, 8409–8421.
- Chang, C.-P., P. A. Harr, and H.-J. Chen, 2005: Synoptic disturbances over the equatorial South China Sea and western Maritime Continent during boreal winter. *Mon. Wea. Rev.*, **133**, 489–503.
- Chen, Guanghua, and C.-H. Sui, 2010: Characteristics and origin of quasi-biweekly oscillation over the western North Pacific during boreal summer. *J. Geophys. Res.*, **115**, D14113, doi:10.1029/2009JD013389.
- Chen, Guixing, W. Li, Z. Yuan, and Z. Wen, 2005: Evolution mechanisms of the intraseasonal oscillation associated with the Yangtze River Basin flood in 1998. *Sci. China Ser. Earth Sci.*, **48**, 957–967.
- Chen, T.-C., and S.-P. Weng, 1998: Interannual variation of the summer synoptic-scale disturbance activity in the western tropical Pacific. *Mon. Wea. Rev.*, **126**, 1725–1733.
- , M. Yen, and S. Weng, 2000: Interaction between the summer monsoons in East Asia and the South China Sea: Intraseasonal monsoon modes. *J. Atmos. Sci.*, **57**, 1373–1392.
- Ding, Y.-H., 1994: *Monsoons over China*. Kluwer Academic, 419 pp.
- , J.-J. Liu, Y. Sun, Y.-J. Liu, H.-H. He, and Y.-F. Song, 2007: A study of the synoptic-climatology of the mei-yu systems in East Asia (in Chinese). *Chin. J. Atmos. Sci.*, **31**, 1082–1101.
- Fujinami, H., and T. Yasunari, 2009: The effects of midlatitude waves over and around the Tibetan Plateau on submonthly variability of the East Asian summer monsoon. *Mon. Wea. Rev.*, **137**, 2286–2304.
- Gilman, D. L., F. J. Fuglister, and J. M. Mitchell Jr., 1963: On the power spectrum of “red noise.” *J. Atmos. Sci.*, **20**, 182–184.
- Gu, G., and C. Zhang, 2001: A spectrum analysis of synoptic-scale disturbances in the ITCZ. *J. Climate*, **14**, 2725–2739.
- , and —, 2002: Westward-propagating synoptic-scale disturbances and the ITCZ. *J. Atmos. Sci.*, **59**, 1062–1075.
- Jiao, M., X. Yao, B. Zhou, and K. Yang, 2004: *Synoptic Analysis of Summer 2003 Heavy Rainfall over Huai River Basin* (in Chinese). China Meteorological Press, 215 pp.
- Lau, K.-H., and N.-C. Lau, 1990: Observed structure and propagation characteristics of tropical summertime synoptic-scale disturbances. *Mon. Wea. Rev.*, **118**, 1888–1913.
- , and —, 1992: The energetics and propagation dynamics of tropical summertime synoptic-scale disturbances. *Mon. Wea. Rev.*, **120**, 2523–2539.
- Liu, H., D.-L. Zhang, and B. Wang, 2008: Daily to submonthly weather and climate characteristics of the summer 1998 extreme rainfall over the Yangtze River basin. *J. Geophys. Res.*, **113**, D22101, doi:10.1029/2008JD010072.
- Mao, J., and G. Wu, 2006: Intraseasonal variations of the Yangtze rainfall and its related atmospheric circulation features during the 1991 summer. *Climate Dyn.*, **27**, 815–830.
- , S. Zhang, and G. Wu, 2010: 20–50-day oscillation of summer Yangtze rainfall in response to intraseasonal variations in the subtropical high over the western North Pacific and South China Sea. *Climate Dyn.*, **34**, 747–761.
- Qian, J.-H., W.-K. Tao, and K.-M. Lau, 2004: Mechanisms for torrential rain associated with the mei-yu development during SCSMEX 1998. *Mon. Wea. Rev.*, **132**, 2–27.
- Simmons, A., S. Uppala, D. Dee, and S. Kobayashi, 2006: ERA-Interim: New ECMWF reanalysis produces from 1989 onwards. *ECMWF Newsletter*, No. 110, Reading, United Kingdom, 26–35.
- Sun, J., J. Wei, X. Zhang, H. Chen, S. Zhao, and S. Tao, 2004: The abnormal weather in the summer 2003 and its real-time prediction (in Chinese). *Climatic Environ. Res.*, **9**, 203–217.
- , H. Zhou, and S. Zhao, 2006: An observational study of mesoscale convective systems producing severe heavy rainfall in

- the Huaihe River basin during 3-4 July 2003 (in Chinese). *Chin. J. Atmos. Sci.*, **30**, 1103–1118.
- Tam, C.-Y., and T. Li, 2006: The origin and dispersion characteristics of the observed tropical summertime synoptic-scale waves over the western Pacific. *Mon. Wea. Rev.*, **134**, 1630–1646.
- Wang, H., and Y. Ni, 2006: Diagnostic analysis and numerical simulation of a mesoscale torrential rain systems in the Huaihe Valley during the rainy season in 2003 (in Chinese). *Acta Meteor. Sin.*, **64**, 734–742.
- Wang, Y.-Q., O. L. Sen, and B. Wang, 2003: A highly resolved regional climate model (IPRC-RegCM) and its simulation of the 1998 severe precipitation event over China. Part I: Model description and verification of simulation. *J. Climate*, **16**, 1721–1738.
- Wu, R., and B. Wang, 2001: Multi-stage onset of the summer monsoon over the western North Pacific. *Climate Dyn.*, **17**, 277–289.
- Yang, H., and C. Li, 2003: The relation between atmospheric intraseasonal oscillation and summer severe flood and drought in the Changjiang–Huaihe River basin. *Adv. Atmos. Sci.*, **20**, 540–553.
- Yang, J., B. Wang, B. Wang, and Q. Bao, 2010: Biweekly and 21–30-day variabilities of the subtropical East Asian monsoon over the lower reach of Yangtze River basin. *J. Climate*, **23**, 1146–1159.
- , Q. Bao, B. Wang, D.-Y. Gong, H. He, and M.-N. Gao, 2013: Distinct quasi-biweekly features of the subtropical East Asian monsoon during early and late summers. *Climate Dyn.*, doi:10.1007/s00382-013-1728-6, in press.
- Yasunari, T., and T. Miwa, 2006: Convective cloud systems over the Tibetan Plateau and their impact on meso-scale disturbances in the Meiyu/Baiu frontal zone: A case study in 1998. *J. Meteor. Soc. Japan*, **84**, 783–803.
- Yatagai, A., P. Xie, and P. Alpert, 2008: Development of a daily gridded precipitation data set for the Middle East. *Adv. Geosci.*, **12**, 165–170.
- , K. Kamiguchi, O. Arakawa, A. Hamada, N. Yasutomi, and A. Kitoh, 2012: APHRODITE: Constructing a long-term daily gridded precipitation dataset for Asia based on a dense network of rain gauges. *Bull. Amer. Meteor. Soc.*, **93**, 1401–1415.
- Zhang, M., and D.-L. Zhang, 2012: Subkilometer simulation of a torrential-rain-producing mesoscale convective system in East China. Part I: Model verification and convective organization. *Mon. Wea. Rev.*, **140**, 184–201.
- Zhang, Q., S. Tao, and S. Zhang, 2003: The persistent heavy rainfall over the Yangtze River valley and its associations with the circulations over East Asian during summer (in Chinese). *Chin. J. Atmos. Sci.*, **27**, 1018–1030.
- Zhang, X., P. Guo, and J. He, 2002: Characteristics of low frequency oscillation of precipitation and wind field in the middle and low reaches of the Yangtze River in summer 1991 (in Chinese). *J. Nanjing Inst. Meteor.*, **25**, 388–394.
- Zhou, Y.-S., S.-T. Gao, and G. Deng, 2005: A diagnostic study of water vapor transport and budget during heavy precipitation over the Changjiang River and the Huaihe River basins in 2003 (in Chinese). *Chin. J. Atmos. Sci.*, **29**, 195–204.
- Zhu, C., T. Nakazawa, J. Li, and L. Chen, 2003: The 30–60 day intraseasonal oscillation over the western North Pacific Ocean and its impacts on summer flooding in China during 1998. *Geophys. Res. Lett.*, **30**, 1952, doi:10.1029/2003GL017817.
- Zhu, Q., J. Lin, S. Shou, and D. Tang, 2000: *The Principles and Methodology of Synoptic Meteorology* (in Chinese). China Meteorological Press, 649 pp.